Coupled-cluster calculations of nucleonic matter

G. Hagen,[1,2] T. Papenbrock,[1,2] A. Ekström,[3,4] K. A. Wendt,[1,2] G. Baardsen,[3] S. Gandolfi,[5]
M. Hjorth-Jensen,[3,4,6] and C. J. Horowitz[7]

[1]*Physics Division, Oak Ridge National Laboratory, Oak Ridge, Tennessee 37831, USA*
[2]*Department of Physics and Astronomy, University of Tennessee, Knoxville, Tennessee 37996, USA*
[3]*Department of Physics and Center of Mathematics for Applications, University of Oslo, N-0316 Oslo, Norway*
[4]*National Superconducting Cyclotron Laboratory, Michigan State University, East Lansing, Michigan 48824, USA*
[5]*Theoretical Division, Los Alamos National Laboratory Los Alamos, New Mexico 87545, USA*
[6]*Department of Physics and Astronomy, Michigan State University, East Lansing, Michigan 48824, USA*
[7]*Indiana University, Bloomington, Indiana 47405, USA*

Background: The equation of state (EoS) of nucleonic matter is central for the understanding of bulk nuclear properties, the physics of neutron star crusts, and the energy release in supernova explosions. Because nuclear matter exhibits a finely tuned saturation point, its EoS also constrains nuclear interactions.

Purpose: This work presents coupled-cluster calculations of infinite nucleonic matter using modern interactions from chiral effective field theory (EFT). It assesses the role of correlations beyond particle-particle and hole-hole ladders, and the role of three-nucleon forces (3NFs) in nuclear matter calculations with chiral interactions.

Methods: This work employs the optimized nucleon-nucleon (NN) potential NNLO$_{\rm opt}$ at next-to-next-to leading order, and presents coupled-cluster computations of the EoS for symmetric nuclear matter and neutron matter. The coupled-cluster method employs up to selected triples clusters and the single-particle space consists of a momentum-space lattice. We compare our results with benchmark calculations and control finite-size effects and shell oscillations via twist-averaged boundary conditions.

Results: We provide several benchmarks to validate the formalism and show that our results exhibit a good convergence toward the thermodynamic limit. Our calculations agree well with recent coupled-cluster results based on a partial wave expansion and particle-particle and hole-hole ladders. For neutron matter at low densities, and for simple potential models, our calculations agree with results from quantum Monte Carlo computations. While neutron matter with interactions from chiral EFT is perturbative, symmetric nuclear matter requires nonperturbative approaches. Correlations beyond the standard particle-particle ladder approximation yield non-negligible contributions. The saturation point of symmetric nuclear matter is sensitive to the employed 3NFs and the employed regularization scheme. 3NFs with nonlocal cutoffs exhibit a considerably improved convergence than their local cousins. We are unable to find values for the parameters of the short-range part of the local 3NF that simultaneously yield acceptable values for the saturation point in symmetric nuclear matter and the binding energies of light nuclei.

Conclusions: Coupled-cluster calculations with nuclear interactions from chiral EFT yield nonperturbative results for the EoS of nucleonic matter. Finite-size effects and effects of truncations can be controlled. For the optimization of chiral forces, it might be useful to include the saturation point of symmetric nuclear matter.

PACS number(s): 21.65.Mn, 21.30.−x, 21.60.De

I. INTRODUCTION

Bulk nucleonic matter is interesting for several reasons. The equation of state (EoS) of neutron matter, for instance, determines properties of supernova explosions [1], and of neutron stars [2–7], and it links the latter to neutron radii in atomic nuclei [8–10] and symmetry energy [11,12]. Likewise, the compressibility of nuclear matter is probed in giant dipole excitations [13], and the symmetry energy of nuclear matter is related to the difference between proton and neutron radii in atomic nuclei [14–16]. The saturation point of nuclear matter determines bulk properties of atomic nuclei, and is therefore an important constraint for nuclear energy-density functionals and mass models (see, e.g., Refs. [17,18]).

The determination and our understanding of the EoS for nuclear matter is intimately linked with our capability to solve the nuclear many-body problem. Here, correlations beyond

the mean field play an important role. Theoretical studies of nuclear matter and the pertinent EoS span back to the very early days of nuclear many-body physics. Early computations are nicely described in the 1967 review by Day [19]. These early calculations were performed using Brueckner-Bethe-Goldstone theory [20,21]; see Refs. [3,22,23] for recent reviews and developments. In these calculations, mainly particle-particle correlations were summed to infinite order. Other correlations were often included in a perturbative way. Coupled-cluster calculations of nuclear matter were performed already during the late 1970s and early 1980s [24,25]. In recent years, there has been a considerable algorithmic development of first-principle methods for solving the nuclear many-body problem. A systematic inclusion of other correlations in a nonperturbative way are nowadays accounted for in Monte Carlo methods [26–30], self-consistent Green's function approaches [23,31–34],

nuclear density functional theory [16,18], and coupled-cluster theory [35,36].

Similar progress has been made in the derivation of nuclear forces based on chiral effective field theory (EFT) [37,38]. Nuclear Hamiltonians from chiral EFT are now used routinely in nucleonic matter calculations, with the three-nucleon forces (3NFs) [39,40] being front and center of many studies [34,41–48]. We note finally that there are also approaches to nucleonic matter based on lattice quantum chromodynamics [49].

In this work we study the EoS of nucleonic matter, using modern NN interactions and 3NFs from chiral EFT, and an implementation of the coupled-cluster method [50,51] that has become a standard in quantum chemistry [52,53]. We employ a Cartesian momentum space basis with periodic boundary conditions, similar to the recent coupled-cluster based calculations of the electron gas [54,55]. Our calculations are based on coupled cluster with doubles (CCD) approximation [56–58]. This is the lowest-order truncation for closed-shell systems in a momentum-space basis, and we will also explore the role of selected triples clusters. We employ a recent parametrization [36] of the NN force from chiral EFT at next-to-next-to-leading order, with inclusion of the 3NF that enters at the same chiral order.

The recent work by Baardsen *et al.* [35] used coupled-cluster theory in the thermodynamic limit, formulated in the relative center-of-mass frame using a partial-wave expansion, to compute the EoS of nuclear matter using modern NN chiral interactions. Baardsen *et al.* [35] summed particle-particle and hole-hole ladders to infinite order (CCD$_{ladd}$), while neglecting particle-hole and other nonlinear terms that enter in the CCD approximation. In this work we include all terms that enter at the CCD cluster truncation level, and we can therefore assess the role of these correlations by comparing to the method developed in [35]. Further, the current implementation of CCD in the laboratory frame using PBC facilitates the inclusion of 3NFs considerably, and we also study effects of selected triples excitations to the EoS.

This paper is organized as follows. In the next section we present the coupled-cluster formalism for infinite matter that includes 3NFs and perturbative triples corrections. The calculations are performed in Cartesian coordinates with a discrete momentum basis and twisted periodic boundary conditions [59–61]. This avoids the tedious partial-wave expansion of the nuclear forces, and it eases considerably the numerical evaluation of 3NFs. Averaging over twisted periodic boundary conditions minimizes finite-size effects and provides us with a good convergence towards the thermodynamic limit. Section II also presents computational results for finite-size effects and a few benchmark calculations. Our results for symmetric nuclear matter and pure neutron matter are presented in Sec. III. Concluding remarks are given in Sec. IV.

II. METHOD

In this section we present the coupled-cluster formalism for infinite matter. We discuss the inclusion and treatment of NN forces and 3NFs from chiral effective field theory (EFT), correlations up to three-particle–three-hole excitations

and finite-size effects. Several benchmark calculations give us confidence in the validity of our approach.

A. Interaction and model space

Our Hamiltonian is

$$H = T_{kin} + V_{NN} + V_{3NF}.$$

Here, T_{kin} denotes the kinetic energy, and V_{NN} and V_{3NF} denote the translationally invariant NN interaction and 3NF. The NN interaction and 3NF are from chiral effective field theory [37,38] at next-to-next-to-leading order (NNLO). We employ the parametrization NNLO$_{opt}$ for the NN interaction [36], and the local 3NF [62]. This 3NF has a local regulator, i.e., the cutoff is in the momentum transfer, and thereby differs from implementations of the 3NF [40] that employ the cutoff in the relative Jacobi momenta. We note that the numerical implementation of the 3NF in the discrete momentum basis is much simpler than in the harmonic oscillator basis commonly used for finite nuclei, because essentially no transformation of matrix elements is necessary. Nevertheless, the sheer number of matrix elements (and associated function calls) of the 3NF is huge, and this is computationally still a limiting factor.

For the model space, we choose a cubic lattice in momentum space with $(2n_{max} + 1)^3$ momentum points. The spin (spin-isospin) degeneracy of each momentum point is $g_s = 2$ ($g_s = 4$) for pure neutron matter (nuclear matter). Thus, filling of the lattice yields shell closures for "Fermi spheres" with $g_s n$ fermions, and $n = 1, 7, 19, 27, 33, 57, \ldots$. We note that one could also use noncubic lattices. Any periodic lattice permits one to implement momentum conservation exactly. For fixed particle number $A = g_s n$ and density $\rho = g_s k_F^3/(6\pi^2)$ (or Fermi momentum k_F), one computes the volume of the cubic box $V = L^3 = A/\rho$, and the box length L that determines the lattice spacing $\Delta k = 2\pi/L$. We note that the computed results exhibit a dependence on the shell closure n. However, Sec. II D shows that shell effects and finite-size effects can be mitigated and controlled, and that the dependence on the parameter n becomes very small.

The second parameter of our lattice is n_{max}. We note that $n_{max}\Delta k$ is the momentum cutoff of our single-particle basis. One has to increase n_{max} until the computed results (e.g., the energy per nucleon) is practically independent of this parameter. For the results reported below we find that $n_{max} = 4$ is sufficient.

B. Coupled-cluster theory for infinite systems

In this section we present the coupled-cluster equations for nucleonic matter. Our calculations of nucleonic matter are based on the recently optimized chiral nucleon-nucleon interaction at NNLO$_{opt}$ [36] with the 3NF at the same chiral order. The low-energy constants (LECs) of the 3NF were determined by fitting the constants c_E and c_D to reproduce the experimental half-life and binding energy of the triton. The optimized 3NF LECs are $c_E = -0.389$ and $c_D = -0.39$. With these values the ^{4}He binding energy is -28.47 MeV [63]. We employ single-particle states

$$|\vec{p}, s_z, t_z\rangle \equiv |\mathbf{k}\rangle,$$

with momentum $\vec{p}$, spin projection s_z and isospin projection t_z. Discrete values of the momentum variable $\vec{p} = \hbar\vec{k}$ result from periodic boundary conditions in a cubic box with length L, that is

$$k_{n_i} = \frac{2\pi n_i}{L}, \quad n_i = 0, \pm 1, \ldots \pm n_{\max}, \quad i = x, y, z.$$

In this basis, the nuclear Hamiltonian with nucleon-nucleon and three-nucleon interactions is

$$
\begin{aligned}
H = & \sum_{pq} \langle \mathbf{k}_p | T_{\text{kin}} | \mathbf{k}_q \rangle a_p^\dagger a_q \\
& + \frac{1}{4} \sum_{pqrs} \langle \mathbf{k}_p \mathbf{k}_q | V_{\text{NN}} | \mathbf{k}_r \mathbf{k}_s \rangle a_p^\dagger a_q^\dagger a_s a_r \\
& + \frac{1}{36} \sum_{pqrstu} \langle \mathbf{k}_p \mathbf{k}_q \mathbf{k}_r | V_{\text{3NF}} | \mathbf{k}_s \mathbf{k}_t \mathbf{k}_u \rangle a_p^\dagger a_q^\dagger a_r^\dagger a_u a_t a_s.
\end{aligned} \tag{1}
$$

The kinetic energy is diagonal in the discrete momentum basis $\langle \mathbf{k}_p | T_{\text{kin}} | \mathbf{k}_q \rangle = \frac{\hbar^2}{2m} \vec{k}_p^2 \delta_{pq}$. The operators $a_p^\dagger$ and a_p create and annihilate a nucleon in state $|\mathbf{k}_p\rangle$, respectively.

The discrete momentum basis allows us to respect translational invariance of the NN potential and the 3NFs. Momentum is conserved, meaning that the two- and three-body matrix elements of the Hamiltonian (1) vanish unless

$$\vec{k}_p + \vec{k}_q = \vec{k}_r + \vec{k}_s,$$

and

$$\vec{k}_p + \vec{k}_q + \vec{k}_r = \vec{k}_s + \vec{k}_t + \vec{k}_u.$$

Note also that the chiral nucleon-nucleon and three-nucleon interactions conserve the total isospin projection, but not the total spin projection.

In single-reference coupled-cluster theory the correlated wave-function is written in the form

$$|\Psi\rangle = e^T |\Phi_0\rangle.$$

Here $|\Phi_0\rangle = \prod_{i=1}^A a_i^\dagger |0\rangle$ is a product state and serves as the reference. The cluster operator T is a linear combination of n-particle–n-hole (np-nh) excitation operators, i.e., $T = T_1 + T_2 + \cdots + T_n$. In the discretized momentum basis the reference state is the closed shell Fermi vacuum, and is obtained by filling the A states with the lowest kinetic energy. We limit ourselves to spin saturated reference state, meaning that each momentum orbital of the reference state is doubly occupied. In this case the nuclear interaction does not induce 1p-1h excitations of the reference state, and we have $T_1 = 0$. Thus, the cluster operator becomes

$$T = \frac{1}{4} \sum_{ijab} \langle \mathbf{k}_a \mathbf{k}_b | t | \mathbf{k}_i \mathbf{k}_j \rangle a_a^\dagger a_b^\dagger a_j a_i + \cdots.$$

Here and in what follows, indices i,j,k,l (a,b,c,d) label occupied (unoccupied) states. Truncating T at the 2p-2h excitation level ($T \approx T_2$) gives the coupled-cluster doubles (CCD) approximation. The CCD energy and amplitude equations can be written in compact form

$$E_{\text{CCD}} = E_0 + \langle \Phi_0 | \overline{H}_N | \Phi_0 \rangle, \tag{2}$$

$$0 = \langle \Phi_{ij}^{ab} | \overline{H}_N | \Phi_0 \rangle. \tag{3}$$

Here

$$
\begin{aligned}
E_0 = & \langle \Phi_0 | H | \Phi_0 \rangle \\
= & \sum_i \langle \mathbf{k}_i | f | \mathbf{k}_i \rangle + \frac{1}{2} \sum_{i,j} \langle \mathbf{k}_i \mathbf{k}_j | v | \mathbf{k}_i \mathbf{k}_j \rangle \\
& + \frac{1}{6} \sum_{ijk} \langle \mathbf{k}_i \mathbf{k}_j \mathbf{k}_k | w | \mathbf{k}_i \mathbf{k}_j \mathbf{k}_k \rangle
\end{aligned} \tag{4}
$$

is the vacuum expectation value (which in the case of no 1p-1h corresponds to the Hartree-Fock energy), $|\Phi_{ij}^{ab}\rangle$ is a 2p-2h excitation of the reference state, and $\overline{H}_N \equiv e^{-T} H_N e^T$ is the similarity transformation of the normal-ordered Hamiltonian:

$$
\begin{aligned}
H_N = & \sum_{pq} \langle \mathbf{k}_p | f | \mathbf{k}_q \rangle : a_p^\dagger a_q : \\
& + \frac{1}{4} \sum_{pqrs} \langle \mathbf{k}_p \mathbf{k}_q | v | \mathbf{k}_r \mathbf{k}_s \rangle : a_p^\dagger a_q^\dagger a_s a_r : \\
& + \frac{1}{36} \sum_{pqrstu} \langle \mathbf{k}_p \mathbf{k}_q \mathbf{k}_r | w | \mathbf{k}_s \mathbf{k}_t \mathbf{k}_u \rangle : a_p^\dagger a_q^\dagger a_r^\dagger a_u a_t a_s : .
\end{aligned} \tag{5}
$$

Here $: a_p^\dagger \cdots a_{p'} \cdots :$ is the normal ordered string of operators with respect to the reference state. The normal-ordered one-body operator is given in terms of the Fock matrix elements

$$
\begin{aligned}
\langle \mathbf{k}_p | f | \mathbf{k}_q \rangle = & \langle \mathbf{k}_p | t | \mathbf{k}_q \rangle + \sum_i \langle \mathbf{k}_p \mathbf{k}_i | V_{\text{NN}} | \mathbf{k}_q \mathbf{k}_i \rangle \\
& + \frac{1}{2} \sum_{ij} \langle \mathbf{k}_p \mathbf{k}_i \mathbf{k}_j | V_{\text{3NF}} | \mathbf{k}_q \mathbf{k}_i \mathbf{k}_j \rangle.
\end{aligned} \tag{6}
$$

The normal-ordered two-body operator has matrix elements

$$
\begin{aligned}
\langle \mathbf{k}_p \mathbf{k}_q | v | \mathbf{k}_r \mathbf{k}_s \rangle = & \langle \mathbf{k}_p \mathbf{k}_q | V_{\text{NN}} | \mathbf{k}_r \mathbf{k}_s \rangle \\
& + \sum_i \langle \mathbf{k}_p \mathbf{k}_q \mathbf{k}_i | V_{\text{3NF}} | \mathbf{k}_i \mathbf{k}_r \mathbf{k}_s \rangle.
\end{aligned} \tag{7}
$$

Finally, the normal-ordered three-body operator w has matrix elements

$$\langle \mathbf{k}_p \mathbf{k}_q \mathbf{k}_r | w | \mathbf{k}_s \mathbf{k}_t \mathbf{k}_u \rangle = \langle \mathbf{k}_p \mathbf{k}_q \mathbf{k}_r | V_{\text{3NF}} | \mathbf{k}_s \mathbf{k}_t \mathbf{k}_u \rangle. \tag{8}$$

In most of this work, we will neglect all elements of w when solving the CCD equations. In this normal-ordered two-body approximation, the 3NF enters in the vacuum expectation value (4), the Fock matrix (6), and the normal-ordered two-body operator (7), but the three-body operator w that changes the orbitals of all three nucleons is neglected.

We note that coupled-cluster theory with full inclusion of 3NFs was worked out in the singles and doubles approximation (CCSD) [64], and very recently with triples corrections included [65].

For an efficient numerical implementation one writes the CCD equations (3) in a factorized (quasilinear) form,

$$0 = \langle \mathbf{k}_a \mathbf{k}_b | v | \mathbf{k}_i \mathbf{k}_j \rangle + P(ab) \sum_c \langle \mathbf{k}_b | \chi | \mathbf{k}_c \rangle \langle \mathbf{k}_a \mathbf{k}_c | t | \mathbf{k}_i \mathbf{k}_j \rangle - P(ij) \sum_k \langle \mathbf{k}_k | \chi | \mathbf{k}_j \rangle \langle \mathbf{k}_a \mathbf{k}_b | t | \mathbf{k}_i \mathbf{k}_k \rangle + \frac{1}{2} \sum_{cd} \langle \mathbf{k}_a \mathbf{k}_b | \chi | \mathbf{k}_c \mathbf{k}_d \rangle \langle \mathbf{k}_c \mathbf{k}_d | t | \mathbf{k}_i \mathbf{k}_j \rangle$$

$$+ \frac{1}{2} \sum_{kl} \langle \mathbf{k}_a \mathbf{k}_b | t | \mathbf{k}_k \mathbf{k}_l \rangle \langle \mathbf{k}_k \mathbf{k}_l | \chi | \mathbf{k}_i \mathbf{k}_j \rangle + P(ij) P(ab) \sum_{kc} \langle \mathbf{k}_a \mathbf{k}_c | t | \mathbf{k}_i \mathbf{k}_k \rangle \langle \mathbf{k}_k \mathbf{k}_b | \chi | \mathbf{k}_c \mathbf{k}_j \rangle$$

$$+ \frac{1}{2} P(ij) \sum_{cdk} \langle \mathbf{k}_a \mathbf{k}_k \mathbf{k}_b | w | \mathbf{k}_i \mathbf{k}_c \mathbf{k}_d \rangle \langle \mathbf{k}_c \mathbf{k}_d | t | \mathbf{k}_k \mathbf{k}_j \rangle - \frac{1}{2} P(ab) \sum_{ckl} \langle \mathbf{k}_a \mathbf{k}_k \mathbf{k}_l | w | \mathbf{k}_i \mathbf{k}_c \mathbf{k}_j \rangle \langle \mathbf{k}_c \mathbf{k}_b | t | \mathbf{k}_k \mathbf{k}_l \rangle. \tag{9}$$

Here, $P(pq) \equiv 1 - P_{pq}$ is an antisymmetrization operator, and we employed the intermediates

$$\langle \mathbf{k}_b | \chi | \mathbf{k}_c \rangle = \langle \mathbf{k}_b | f | \mathbf{k}_c \rangle - \frac{1}{2} \sum_{kld} \langle \mathbf{k}_b \mathbf{k}_d | t | \mathbf{k}_k \mathbf{k}_l \rangle \langle \mathbf{k}_k \mathbf{k}_l | v | \mathbf{k}_c \mathbf{k}_d \rangle + \frac{1}{4} \sum_{edkl} \langle \mathbf{k}_k \mathbf{k}_l \mathbf{k}_b | w | \mathbf{k}_e \mathbf{k}_d \mathbf{k}_c \rangle \langle \mathbf{k}_e \mathbf{k}_d | t | \mathbf{k}_k \mathbf{k}_l \rangle, \tag{10}$$

$$\langle \mathbf{k}_k | \chi | \mathbf{k}_j \rangle = \langle \mathbf{k}_k | f | \mathbf{k}_j \rangle + \frac{1}{2} \sum_{kcd} \langle \mathbf{k}_k \mathbf{k}_l | v | \mathbf{k}_c \mathbf{k}_d \rangle \langle \mathbf{k}_c \mathbf{k}_d | t | \mathbf{k}_j \mathbf{k}_l \rangle + \frac{1}{4} \sum_{cdln} \langle \mathbf{k}_l \mathbf{k}_n \mathbf{k}_k | w | \mathbf{k}_c \mathbf{k}_d \mathbf{k}_j \rangle \langle \mathbf{k}_c \mathbf{k}_d | t | \mathbf{k}_l \mathbf{k}_n \rangle, \tag{11}$$

$$\langle \mathbf{k}_k \mathbf{k}_l | \chi | \mathbf{k}_i \mathbf{k}_j \rangle = \langle \mathbf{k}_k \mathbf{k}_l | v | \mathbf{k}_i \mathbf{k}_j \rangle + \frac{1}{2} \sum_{cd} \langle \mathbf{k}_k \mathbf{k}_l | v | \mathbf{k}_c \mathbf{k}_d \rangle \langle \mathbf{k}_c \mathbf{k}_d | t | \mathbf{k}_i \mathbf{k}_j \rangle + \frac{1}{2} P(ij) \sum_{cdn} \langle \mathbf{k}_n \mathbf{k}_k \mathbf{k}_l | w | \mathbf{k}_c \mathbf{k}_d \mathbf{k}_j \rangle \langle \mathbf{k}_c \mathbf{k}_d | t | \mathbf{k}_n \mathbf{k}_i \rangle, \tag{12}$$

$$\langle \mathbf{k}_k \mathbf{k}_b | \chi | \mathbf{k}_c \mathbf{k}_j \rangle = \langle \mathbf{k}_k \mathbf{k}_b | v | \mathbf{k}_c \mathbf{k}_j \rangle + \sum_{ld} \langle \mathbf{k}_k \mathbf{k}_l | v | \mathbf{k}_c \mathbf{k}_d \rangle \langle \mathbf{k}_c \mathbf{k}_d | t | \mathbf{k}_l \mathbf{k}_j \rangle - \frac{1}{2} \sum_{dln} \langle \mathbf{k}_l \mathbf{k}_k \mathbf{k}_n | w | \mathbf{k}_d \mathbf{k}_j \mathbf{k}_c \rangle \langle \mathbf{k}_d \mathbf{k}_b | t | \mathbf{k}_l \mathbf{k}_n \rangle$$

$$+ \frac{1}{2} \sum_{del} \langle \mathbf{k}_l \mathbf{k}_k \mathbf{k}_b | w | \mathbf{k}_d \mathbf{k}_e \mathbf{k}_c \rangle \langle \mathbf{k}_d \mathbf{k}_e | t | \mathbf{k}_l \mathbf{k}_j \rangle, \tag{13}$$

$$\langle \mathbf{k}_a \mathbf{k}_b | \chi | \mathbf{k}_c \mathbf{k}_d \rangle = \langle \mathbf{k}_a \mathbf{k}_b | v | \mathbf{k}_c \mathbf{k}_d \rangle - \frac{1}{2} P(ab) \sum_{ekl} \langle \mathbf{k}_k \mathbf{k}_l \mathbf{k}_b | w | \mathbf{k}_e \mathbf{k}_c \mathbf{k}_d \rangle \langle \mathbf{k}_e \mathbf{k}_a | t | \mathbf{k}_k \mathbf{k}_l \rangle. \tag{14}$$

In Eqs. (9)–(14) the numerically expensive sums that involve products of two-body operators can all be implemented efficiently as matrix-matrix multiplications. The momentum conservation reduces the computational cost of the CCD equations to $n_o n_u^3$, where n_o (n_u) is the number of occupied (unoccupied) momentum states. This is a considerable reduction in computational cycles as compared to the normal cost of the CCD equations which is $n_o^2 n_u^4$ [52], and similar to the reduction of computational cost achieved in the angular momentum coupled scheme [66,67].

The coupled-cluster equations (9) are solved numerically by iteration and yield the matrix elements of T_2. The CCD energy (2) is given in algebraic form by

$$E_{\text{CCD}} = E_0 + \frac{1}{4} \sum_{ijab} \langle \mathbf{k}_i \mathbf{k}_j | v | \mathbf{k}_a \mathbf{k}_b \rangle \langle \mathbf{k}_a \mathbf{k}_b | t | \mathbf{k}_i \mathbf{k}_j \rangle.$$

Below, we will also employ an approximation (denoted as CCD$_{\text{ladd}}$) that only uses the particle-particle and hole-hole ladders in the CCD equations, i.e.,

$$0 = \langle \mathbf{k}_a \mathbf{k}_b | v | \mathbf{k}_i \mathbf{k}_j \rangle$$
$$+ P(ab) \sum_c \langle \mathbf{k}_b | f | \mathbf{k}_c \rangle \langle \mathbf{k}_a \mathbf{k}_c | t | \mathbf{k}_i \mathbf{k}_j \rangle$$
$$- P(ij) \sum_k \langle \mathbf{k}_k | f | \mathbf{k}_j \rangle \langle \mathbf{k}_a \mathbf{k}_b | t | \mathbf{k}_i \mathbf{k}_k \rangle$$

$$+ \frac{1}{2} \sum_{cd} \langle \mathbf{k}_a \mathbf{k}_b | v | \mathbf{k}_c \mathbf{k}_d \rangle \langle \mathbf{k}_c \mathbf{k}_d | t | \mathbf{k}_i \mathbf{k}_j \rangle$$
$$+ \frac{1}{2} \sum_{kl} \langle \mathbf{k}_a \mathbf{k}_b | t | \mathbf{k}_k \mathbf{k}_l \rangle \langle \mathbf{k}_k \mathbf{k}_l | v | \mathbf{k}_i \mathbf{k}_j \rangle. \tag{15}$$

The CCD$_{\text{ladd}}$ approximation was used in Ref. [35] within coupled-cluster theory, and a similar approximation was also employed in other computations of nucleonic matter, see, e.g., Refs. [42,43].

Let us also discuss the inclusion of three-body clusters. When going beyond the CCD approximation and considering triples excitations, one might question whether the residual three-body part w can safely be neglected. After all, three-body forces directly induce excitations of three-body clusters. Below we will include the residual part w when considering contributions from triples excitations to the correlation energy, and study the accuracy of the normal-ordered two-body approximation in the presence of triples excitations in neutron and symmetric nuclear matter. Very recently, Binder *et al.* employed chiral interactions softened via the similarity renormalization group transformation [68,69], studied the effect of triples corrections in the presence of 3NFs in nuclei such as ^{16}O and ^{40}Ca, and found it to be small [65].

The full inclusion of triples in the presence of three-body forces is demanding and computationally expensive. Some effects of triples can be included in the CCD(T) approximation [70] that we extend to 3NFs. In CCD(T) the

triples excitation amplitude is approximated as

$$t_{ijk}^{abc} \equiv \langle \mathbf{k}_a \mathbf{k}_b \mathbf{k}_c | t | \mathbf{k}_i \mathbf{k}_j \mathbf{k}_k \rangle$$
$$\approx \langle \Phi_{ijk}^{abb} | (v + w)(1 + \hat{T}_2) | \Phi_0 \rangle / \epsilon_{abc}^{ijk}. \qquad (16)$$

Here

$$\epsilon_{abc}^{ijk} \equiv f_i^i + f_j^j + f_k^k - f_a^a - f_b^b - f_c^c. \qquad (17)$$

The CCD(T) correction to the energy is

$$\Delta E_{\text{CCD(T)}} = \frac{1}{36} \sum_{ijkabc} |t_{ijk}^{abc}|^2 / \epsilon_{abc}^{ijk}. \qquad (18)$$

Employing the triples amplitude (16) with the inclusion of w yields the energy correction $\Delta E_{\text{CCD(T)}}$. We also consider the following approximations. Neglecting the residual three-body part w yields the normal-ordered two-body approximation to the CCD(T) energy correction, denoted as $\Delta E_{\text{CCD(T):}w=0}$. Omitting the term wT_2 in Eq. (16) gives the energy correction $\Delta E_{\text{CCD(T):}wT_2=0}$. Note that the numerically expensive term wT_2 in Eq. (16) consist of three distinct diagrams in which one sums over pp, hh, and ph intermediate states, respectively. Below we will investigate the contributions of these three diagrams to the CCD(T) energy correction in neutron and symmetric nuclear matter.

C. Ladder approximation in a partial-wave basis

In Ref. [35], the ladder approximation of the coupled-cluster equations for nuclear matter is presented in an alternative formulation. Historically, the equations for nuclear matter, for example in the hole-line approximation [71], have often been expressed explicitly in a partial-wave basis [72–74]. Similarly, in the method presented in Ref. [35], the ladder approximation is formulated in a partial-wave basis, assuming that the thermodynamic limit is reached and therefore using integrals over relative and center-of-mass momenta. In the partial-wave expanded equations, the Pauli exclusion operators are treated exactly, using a technique introduced for the Brueckner-Hartree-Fock approximation by Suzuki *et al.* [74]. Apart from the truncation in partial waves, the only approximation in this method is in the single-particle potentials, where an angular-average approximation was used for the laboratory momentum argument [35,75].

D. Finite-size effects

We would like to quantify the error due to finite-size effects and the accuracy of our coupled-cluster calculations of neutron and nuclear matter. Using periodic boundary conditions (PBC) one could increase the number of particles in the box until convergence to the thermodynamic limit is reached. However, due to variations of the shell effects at different closed shell configurations, there is no guarantee that increasing the number of particles will lead to a systematic and smooth convergence to the thermodynamic limit. Furthermore, the computational cost of many-body methods such as the AFDMC and coupled-cluster methods increases rapidly with increasing particle number, and one would therefore like to employ a method that controls finite-size effects already for

modest particle numbers. This can be achieved with averaging over phases of Bloch waves that correspond to different boundary conditions [59–61].

Consider a free particle in a box of size L subject to twisted boundary condition, that is, the wave function with momentum k fulfills the condition for so-called Bloch waves, namely, $\psi_k(x + L) = e^{i\theta} \psi_k(x)$. By averaging over the twist angle θ, shell effects can be eliminated for free Fermi systems [59], and they are much suppressed for interacting systems [60,61]. In this way, one obtains a much more systematic and smooth convergence towards the thermodynamic limit. The twisted boundary conditions are defined by

$$k_{n_i} = \frac{(2\pi n_i + \theta_i)}{L}, \quad n_i = 0, \pm 1, \ldots \pm n_{\max}, \ i = x, y, z,$$

with the twist angle $\theta \in [0, \pi]$ for systems with time-reversal invariance [61]. This amounts to letting the particles pick up a complex phase when they wrap around the boundary of the cubic box. By integrating or averaging over a finite number of twists in each x, y, z direction we obtain the twist-averaged boundary conditions (TABC). In our implementation of TABC we integrate over the twist angles θ using a finite number of Gauss-Legendre quadrature points in $[0, \pi]$. Note that $\theta = 0$ ($\theta = \pi$) corresponds to (anti)periodic boundary conditions.

In order to quantify the finite-size effects using PBC and TABC we compute the kinetic and potential energy contribution to the Hartree-Fock energy for several closed shell configurations ranging from tens to several hundreds of nucleons, and compare with the thermodynamic limit for these quantities. In Fig. 1 we show the relative error of the kinetic energy in pure neutron matter for the Fermi momentum $k_F = 1.6795 \text{ fm}^{-1}$ computed using standard PBC and TABC. We used 10 Gauss-Legendre points for the twist angle θ_i of the $i = x, y, z$ direction in the integration interval $[0, \pi]$. Clearly, we obtain a much faster and smoother convergence to the thermodynamic limit using TABC. Generally we get about an order of magnitude reduction in the relative error when using
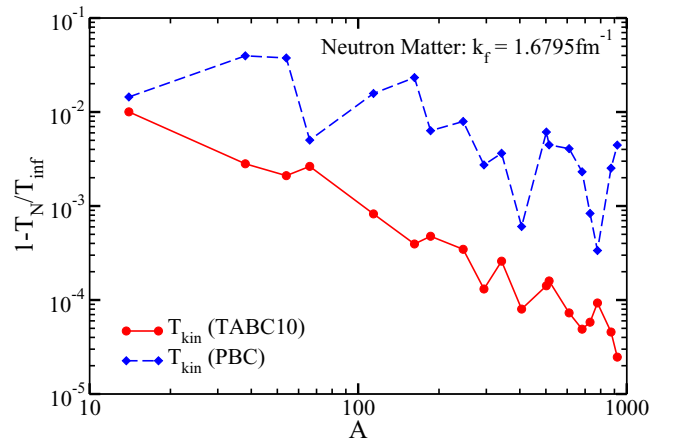

FIG. 1. (Color online) Relative finite-size corrections for the kinetic energy in pure neutron matter at the Fermi momentum $k_F = 1.6795 \text{ fm}^{-1}$ vs the neutron number A. TABC10 are twist-averaged boundary conditions with 10 Gauss-Legendre points in each spatial direction.
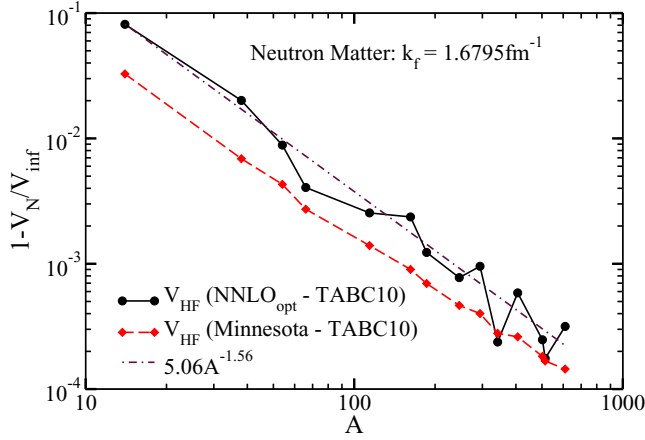
FIG. 2. (Color online) Relative finite-size corrections for the Hartree-Fock energy of the $NNLO_{opt}$ (full line) and Minnesota (dashed line) potentials in pure neutron matter at the Fermi momentum $k_F = 1.6795$ fm^{-1} vs the neutron number A. TABC10 are twist-averaged boundary conditions with 10 Gauss-Legendre points in each spatial direction. The dashed-dotter line shows a power law fit to the $NNLO_{opt}$ results.

FIG. 3. (Color online) Relative finite-size corrections for the Hartree-Fock energy of the NN potential $NNLO_{opt}$ and the 3NF potential in symmetric nuclear matter at the Fermi momentum $k_F = 1.6$ fm^{-1} vs the nucleon number A. PBC: periodic boundary conditions. TABC10 and TABC3 are twist-averaged boundary conditions with 10 and 3 Gauss-Legendre points in each spatial direction, respectively.

TABC as compared to PBC. Finite size effects are particularly small for PBC and $N = 66$ neutrons. This was also seen in AFDMC calculations [27].

Figure 2 shows the relative error of the potential energy to the Hartree-Fock energy in pure neutron matter for the Fermi momentum $k_F = 1.6795$ fm^{-1} computed with TABC. We compute the potential energy from $NNLO_{opt}$ and from the Minnesota potential. We see that the finite-size effects in the potential energy are comparable to the finite-size effects in the kinetic energy shown in Fig. 1. We note that finite-size effects vanish as the power law $A^{-1.56}$ in the neutron number A.

Finally, we would also like to assess the finite-size effects in symmetric nuclear matter. In Fig. 3 we show the relative error of the potential energy to the Hartree-Fock energy in symmetric nuclear matter for the Fermi momentum $k_F = 1.6$ fm^{-1} computed using PBC and TABC. We consider the Hartree-Fock potential energy contribution from the nucleon-nucleon interaction $NNLO_{opt}$ and the 3NF at order NNLO separately. In particular it is seen that the relative error in the potential energy contribution from the 3NF is about an order of magnitude smaller than the relative error coming from the nucleon-nucleon interaction alone using both PBC and TABC. In the case of symmetric nuclear matter there is no systematic convergence trend using PBC, and for 132 nucleons the relative error for PBC is around ∼4%, while using TABC the error is reduced to ∼1%. It is interesting to note that finite size effects for $NNLO_{opt}$ with TABC decrease as $A^{-1.59}$ with increasing nucleon number A. This exponent is similar to the exponent found in neutron matter (see Fig. 2).

Coupled-cluster calculations of nucleonic matter using TABC are very expensive. Using 10 twist angles in each direction requires 10^3 coupled-cluster calculations, although symmetry considerations can reduce this number considerably. In Ref. [61] it was shown that one can find a specific choice of twist angles (known as special points), in which the Hartree-
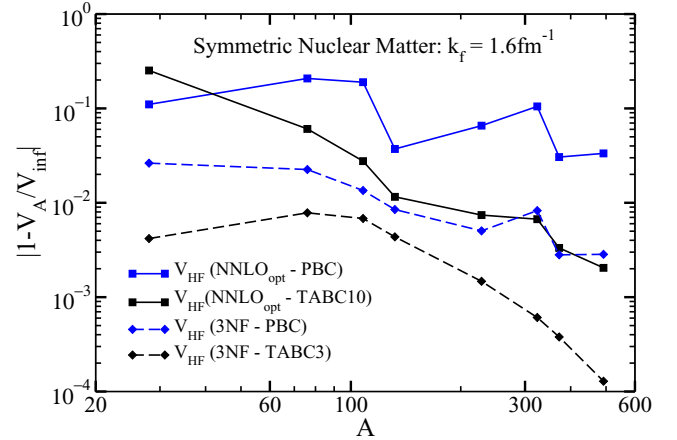
Fock energy exactly corresponds to the Hartree-Fock energy in the thermodynamic limit. In the following we compute these special points for neutron and nuclear matter using both NN interactions and 3NFs, and compare with calculations using PBC and TABC.

E. Benchmarks

It is interesting to compare the results for various boundary conditions with the infinite matter results by Baardsen *et al.* [35]. Figure 4 shows the CCD_{ladd} results for neutron matter computed with the nucleon-nucleon potential $NNLO_{opt}$. In a finite system, the neutron number $N = 66$ is very close to
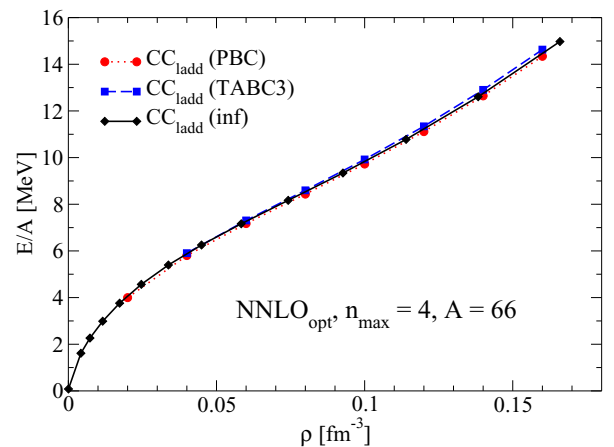

FIG. 4. (Color online) Energy per particle of neutron matter for $NNLO_{opt}$ computed in the CCD_{lad} approximation with periodic boundary conditions (circles), twist-averaged boundary conditions (squares), and for infinite matter (diamonds). The latter results are from Ref. [36]. The calculations used $A = 66$ neutrons and $n_{max} = 4$.
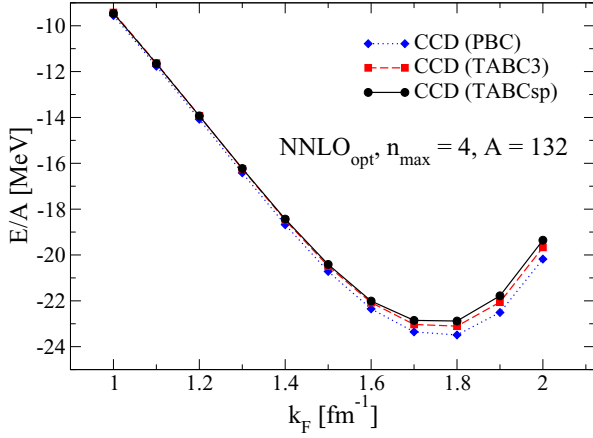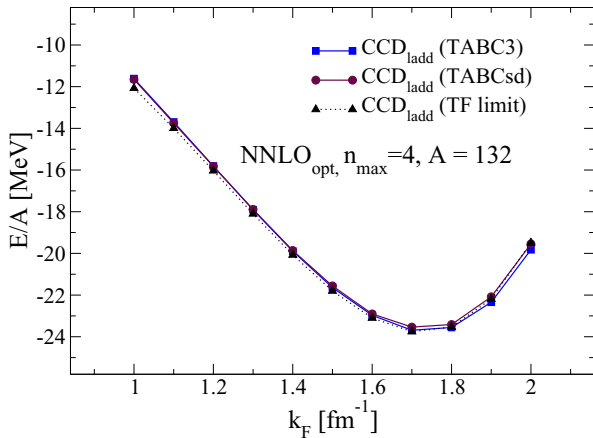
FIG. 5. (Color online) Energy per particle of symmetric nuclear matter for NNLO$_{opt}$ computed in the CCD approximation with periodic boundary conditions (diamonds), twist-averaged boundary conditions (squares), and with a special point and twisted boundary conditions (circles). The calculations used $A = 132$ nucleons and $n_{max} = 4$.

the infinite matter results for both periodic and twist-averaged boundary conditions.

For symmetric nuclear matter, the CCD results are more sensitive to the choice of the boundary conditions, with results shown in Fig. 5. At higher Fermi momenta ($k_F > 1.6$ fm^{-1}), the energy per nucleon for periodic boundary conditions differs by ~0.5 MeV from the result obtained with twist-averaged boundary conditions. A calculation with a special point in the twist is very close to the twist-averaged results. However, for Fermi momenta $k_F < 1.6$ fm^{-1}, the difference between the PBC and TABC is less than 200 keV per nucleon.

Figure 6 compares nuclear matter results calculated in the ladder approximation with the CC$_{ladd}$ of Ref. [35]. The latter were obtained by taking the thermodynamic limit in the relative and center-of mass frame and by summing over partial

FIG. 6. (Color online) Energy per particle of symmetric nuclear matter for NNLO$_{opt}$ computed in the CCD$_{ladd}$ approximation in the thermodynamic limit using partial-wave expansion (triangles) (partly adapted from Ref. [35]), with twist averaged boundary conditions (squares), and with a special point and twisted boundary conditions (circles). The calculations used $A = 132$ nucleons and $n_{max} = 4$.
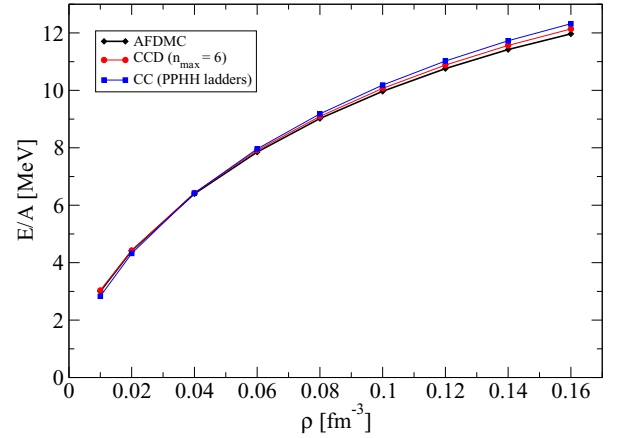

FIG. 7. (Color online) Energy per particle of neutron matter, computed with the Minnesota potential. Diamonds: AFDMC, circles: CCD, squares: CCD limited to pp and hh ladders.

waves. The summation over intermediate particle-particle and hole-hole configurations is performed with an exact Pauli operator, while the single-particle energies are computed using an angle-averaging procedure, see Ref. [35] for further details. For these results, the angle-average approximation, together with a truncation in the number of partial waves included, represent the sources of possible errors in the thermodynamic limit. It is therefore very satisfactory that the results from different methods are close to each other.

Let us also consider a simple potential model and benchmark the results of our coupled-cluster calculations against virtually exact results from the auxiliary field diffusion Monte Carlo (AFDMC) method [76]. The Minnesota potential [77] is a semirealistic nucleon-nucleon interaction that can be solved accurately with AFDMC. It depends only on the relative momenta and spin, but lacks spin-orbit or tensor contributions. The matrix elements of this potential are real numbers. For the benchmark we employ periodic boundary conditions, $A = 66$ neutrons, and $n_{max} = 6$.

Figure 7 compares the energy per neutron of our lattice CCD results (circles), and our CCD$_{ladd}$ in the thermodynamic limit, see Ref. [35], to the AFDMC benchmark. Overall, the agreement is good between all methods. As expected, the CCD results are more accurate than the CCD$_{ladd}$ approximation.

Finally, we turn to 3NFs. The inclusion of 3NFs—even in the normal-ordered approximation—is still numerically expensive due to the large number of required matrix elements. We also study different approximations for 3NFs, and compare the results for symmetric nuclear matter when 3NFs only enter in the normal-ordered approximation as zero-body, one-body, or up to two-body forces. Figure 8 clearly shows that normal-ordered two-body forces are relevant.

III. RESULTS FOR CHIRAL INTERACTIONS

In this section, we present our results for coupled-cluster computations of neutron matter and symmetric nuclear matter. As shown in the previous section, the finite size effects (and the differences between PBC and TABC) are small for
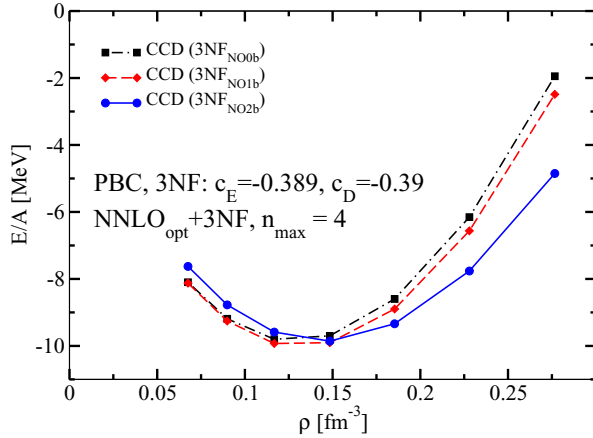
FIG. 8. (Color online) Energy per particle of symmetric nuclear matter computed in the CCD approximation with $NNLO_{opt} + 3NF$ ($c_E = -0.389$, $c_D = -0.39$). The 3NF is included in the zero-body (black dashed-dotted line), one-body (red dashed line), and in the two-body (blue solid line) normal-ordered approximations. The calculations used $A = 132$ nucleons and $n_{max} = 4$.

$A = 66$ neutrons and $A = 132$ nucleons when calculating neutron matter and symmetric nuclear matter, respectively. For this reason, many of the expensive calculations involving 3NFs are only performed with PBC at these specific particle numbers.

A. Neutron matter

Figure 9 shows the energy per neutron as a function of density based on NN interactions alone and compares various many-body methods. The employed NN interaction $NNLO_{opt}$ is perturbative in neutron matter, with second-order many-body perturbation theory (MBPT2), CCD and CCD_{ladd} giving
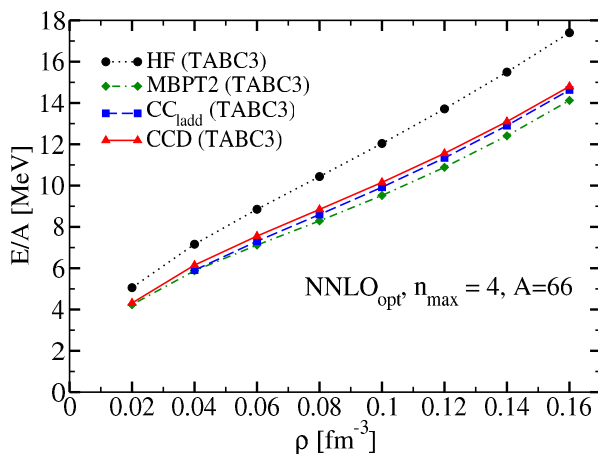
FIG. 9. (Color online) Energy per particle in neutron matter with $NNLO_{opt}$ (NN only). The black dashed line is Hartree-Fock (HF), the green dashed-dotted line is second-order many-body perturbation theory (MBPT2), the blue dashed line is coupled-cluster doubles ladder approximation (CCD_{ladd}), and the red solid line is coupled-cluster doubles (CCD). The calculations used $A = 66$ neutrons, $n_{max} = 4$, and TABC3.
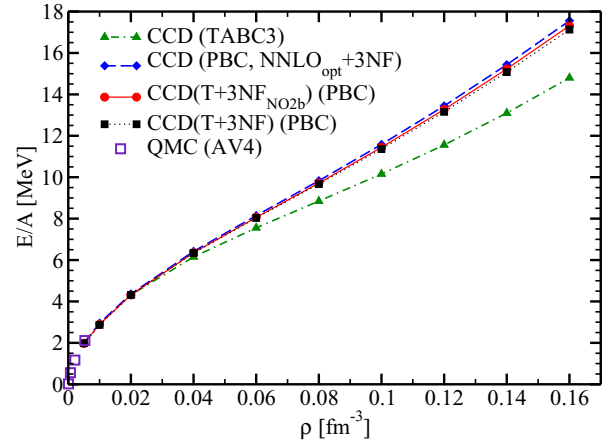

FIG. 10. (Color online) Energy per particle in neutron matter with $NNLO_{opt}$ (NN only) and with inclusion of 3NF computed in the CCD and CCD(T) approximations. The 3NF LECs are given by $c_E = -0.389$ and $c_D = -0.39$. The calculations used $A = 66$ neutrons, $n_{max} = 4$, and PBC and TABC. The QMC results are from Refs. [28,30].

similar results that differ by less than 1 MeV per neutron at nuclear saturation density.

Figure 10 shows the effect of 3NFs in CCD calculations of the EoS for neutron matter. We consider several approximations involving 3NFs, and it is seen that they yield very similar results. We note that three-nucleon forces act repulsively. The results for neutron matter reported here are consistent with the recent calculations of Krueger *et al.* [46], and our results for the EoS fall within their NNLO uncertainty band. The CCD calculation that includes the normal-ordered 3NFs is shown as diamonds. Triples corrections that are limited to the inclusion of up to two-body terms from the normal-ordered 3NF are shown as circles, while triples corrections that include also the residual 3NF are shown as squares. For neutron matter, the effects of triples are small and account for about 0.3 MeV per neutron at high densities, and the residual 3NFs contribute little to the triples corrections. At very low densities, the coupled-cluster results are in agreement with results from quantum Monte Carlo (QMC) calculations [27,28,30,78]. In this low-density regime the physics is dominated by the large scattering length, and the EoS becomes independent of the short-ranged parts of the nuclear interaction.

B. Nuclear matter

In this subsection we perform coupled-cluster calculations of symmetric nuclear matter using chiral NN and 3NF interactions at NNLO. Figure 11 shows the energy per nucleon in symmetric nuclear matter for a wide range of densities computed in MBPT2, the CCD_{ladd}, and in the CCD approximation with the NN potential $NNLO_{opt}$. In these calculations we used $A = 132$ nucleons, $n_{max} = 4$, and TABC based on 3^3 angles. We observe that the saturation point is at a too-large density, and we get a considerable overbinding. These results for $NNLO_{opt}$ are in good agreement with the recent self-consistent Green's function (SCGF) calculations
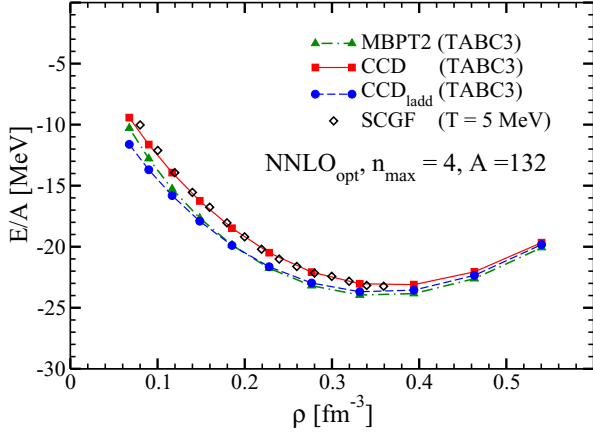
FIG. 11. (Color online) Energy per particle in symmetric nuclear matter with NNLO$_{opt}$ (NN only) computed in the MBPT2 (triangles with green dashed-dotted line), CCD$_{ladd}$ (circles with blue dashed line), and CCD (squares with solid red line) approximations. The calculations used 132 nucleons, $n_{max} = 4$, and TABC3. Diamonds are results from self-consistent Green's function (SCGF) at the finite temperature $T = 5$ MeV, taken from Ref. [34].

FIG. 12. (Color online) Energy per particle in symmetric nuclear matter with NNLO$_{opt}$ and 3NF computed in the MBPT2 (squares with green dashed-dotted line), CCD (circles with blue dashed line), and CCD(T) with 3NF in the normal-ordered two-body approximation (diamonds with solid red line), and including the residual 3NF in leading order (triangles with dotted black line). The 3NF LECs are given by $c_E = -0.389$ and $c_D = -0.39$. The calculations used 132 nucleons, $n_{max} = 4$, and PBC.

of nuclear matter [34], and the CCD$_{ladd}$ calculations of Ref. [35]. The difference between MBPT2 and CCD is about 2 MeV below saturation energy and about three times as large as for neutron matter. The difference between the CCD$_{ladd}$ approximation and the full CCD calculations is around 1 MeV per nucleon around saturation density. We can conclude that—in contrast to neutron matter—for nuclear matter and the NNLO$_{opt}$ interaction (which is rather soft), nonlinear terms in the T_2 amplitude and particle-hole excitations yield non-negligible contributions. These results indicate that nuclear matter for the NNLO$_{opt}$ chiral interaction is not perturbative. We note also that the coupled-cluster calculations are difficult to converge for Fermi momenta smaller than about 0.8 fm^{-1}. This is presumably due to the clustering of nuclear matter at low densities [79]. We also note that the results shown Fig. 11 at high densities are beyond the presumed valididy of the underlying EFT.

Let us turn to 3NFs. Figure 12 shows the energy per nucleon in symmetric nuclear matter for a wide range of densities computed with MBPT2, CCD, and the CCD(T) approximation. The CCD calculations included the 3NF in the normal-ordered two-body approximation. The CCD(T) calculations were performed with 3NFs in the normal-ordered two-body approximation [CCD(T+3NF$_{NO2b}$)], and going beyond the normal-ordered two-body approximation by including the leading-order residual 3NF contribution to the perturbative estimate for the T_3 amplitude [CCD(T+3NF$_{NO3b}$)]. In these calculations we used $A = 132$ nucleons with PBC and $n_{max} = 4$. For the densities we consider here, the difference between PBC and TABC is small.

In contrast to calculations of neutron matter, the contribution from the perturbative triples corrections is sizable in nuclear matter, and about 1 MeV per nucleon in the range of densities shown when including the 3NF in the normal-ordered two-body approximation. Furthermore, we find that the contri-
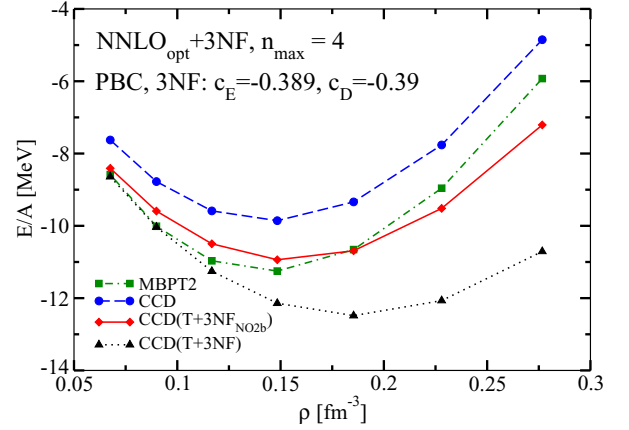
bution of the residual 3NF to the CCD(T) energy is significant around saturation density, indicating that the normal-ordered two-body approximation for the 3NF might not be sufficient in symmetric nuclear matter. We checked that the contribution of the residual 3NF to the CCD amplitude equations is negligible, and therefore it might be sufficient to include the full 3NF in the perturbative triples amplitude. In order to check the accuracy of the perturbative triples approximation [CCD(T)] in nuclear matter we also performed non-perturbative, iterative CCDT-1 (see Refs. [80,81]) calculations for $A = 28$ and $n_{max} = 3$ at two different densities $k_F = 1.3$ fm^{-1} and $k_F = 1.6$ fm^{-1}. We found that the difference between CCD(T) and CCDT-1 in this range of densities is at most 0.1 MeV per nucleon. Therefore, we conclude that the CCD(T) approximation is accurate for the NN potential NNLO$_{opt}$ and chiral 3NFs in symmetric nuclear matter.

C. Scheme dependence of three-nucleon forces

In this subsection, we try to further illuminate the role of 3NFs in nucleonic matter. We study different regularization schemes, and compute the energy per particle in pure neutron matter and symmetric nuclear matter. The 3NF employed in the previous subsections exhibits a cutoff of $\Lambda = 500$ MeV. This cutoff is in the momentum transfer, and therefore local in position space [62]. This choice of regulator for the 3NF is different from the regularization scheme that is used in the nucleon-nucleon sector, and from other regularizations of the 3NF that exhibit cutoffs on Jacobi momenta [40]. We note that regulators that cut off initial and final Jacobi momenta lead to nonlocal interactions. Here, the cutoff function is

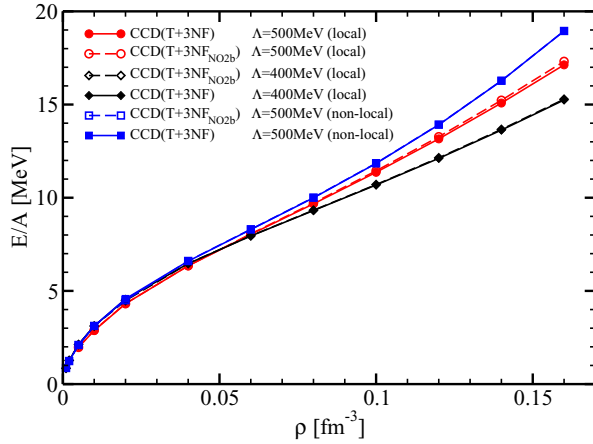$$f_R(\vec{p}, \vec{q}) = \exp\left[-\left(\frac{4p^2 + 3q^2}{4\Lambda^2}\right)^n\right],$$

FIG. 13. (Color online) Energy per particle in pure neutron matter with NNLO$_{opt}$ and 3NF computed in the CCD(T) approximation including 3NFs in the normal ordered two-body approximation and including the residual 3NF in the CCD(T: $wT_2 = 0$) approximation. For the 3NF we used a local regulator with cutoffs $\Lambda = 400$ and $\Lambda = 500$ MeV. The 3NF LECs are given by $c_E = -0.389$ and $c_D = -0.39$ for the $\Lambda = 500$ MeV local regulator, while for the $\Lambda = 400$ MeV local regulator we used $c_E = -0.27$ and $c_D = -0.39$ with c_E adjusted to the ^{4}He binding energy. For the nonlocal regulator with $\Lambda = 500$ MeV cutoff we used $c_E = -0.791$ and $c_D = -2$ adjusted to the triton and ^{3}He binding energies. The calculations used 66 neutrons, $n_{max} = 4$, and PBC.

with $\vec{p} = (\vec{k}_1 - \vec{k}_2)/2$ and $q = [\vec{k}_3 - (\vec{k}_1 - \vec{k}_2)/2](2/3)$. This regulator reduces to the regulator used in the NN sector for $\vec{q} = 0$. In the NN potential NNLO$_{opt}$ we use $n = 3$, while for the local regulator of the 3NF defined in Ref. [62] we use $n = 2$ in the exponential. In what follows, we compare the NNLO$_{opt}$ interaction with a 3NF that also uses a local regulator but a lower cutoff of $\Lambda = 400$ MeV, and with a 3NF that employs a nonlocal regulator and a cutoff $\Lambda = 500$ MeV in relative Jacobi momenta.

Figure 13 shows the energy per particle in pure neutron matter computed in the CCD(T) approximation. Here we included 3NFs in the normal ordered two-body approximation, and in the CCD(T: $wT_2 = 0$) approximation. For the latter, we went beyond the normal ordered two-body approximation and included the residual three-body term w that enters at first order in the triples equation for T_3. In neutron matter the contribution from the residual 3NF w to the energy per particle is small. This indicates that the normal-ordered two-body approximation works very well. In the EoS calculation with the local regulator and the lower cutoff $\Lambda = 400$ MeV we adjusted the LECs of the three-body contact term to $c_E = -0.27$ and kept c_D unchanged. Then, the binding energies of the triton and the nuclei ^{3,4}He are close to the experimental values. For the nonlocal regulator with cutoff $\Lambda = 500$ and power $n = 2$ in the exponential, the LECs $c_E = -0.791$ and $c_D = -2$ reproduce the triton and ^{3}He binding energies. In pure neutron matter the contributions from the 3NF contact terms with the LECs c_E and c_D vanish for a nonlocal regulator, and the contribution to the EoS depends only on the pion-nucleon couplings c_1 and c_3 of the long-range two-pion exchange term
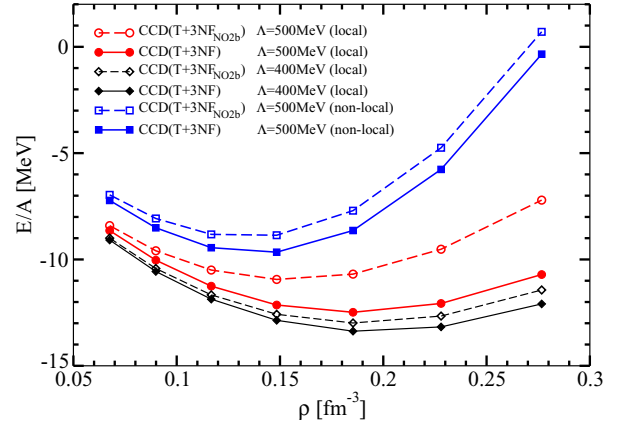

FIG. 14. (Color online) Same caption as in Fig. 13, except that the energy per particle is for symmetric nuclear matter. The calculations used 132 nucleons, $n_{max} = 4$, and PBC.

of the 3NF [42]. However, for a local regulator the 3NF contact terms do not vanish in neutron matter [29]. The results for the EoS for pure neutron matter show a regulator dependence at densities beyond $\rho = 0.08$ fm^{-3}. The band obtained from the different 3NF regulators are within the corresponding band for neutron matter obtained in Ref. [46].

Figure 14 shows the corresponding plot for the energy per particle in symmetric nuclear matter. Here the results for the local regulator with a cutoff $\Lambda = 500$ MeV exhibit a considerable enhancement of the contribution from the residual 3NF w to the energy per particle at densities above the saturation densities. The sizeable triples contribution of the residual 3NF w questions the usually observed hierarchy of the coupled-cluster approximation. The results from the lower cutoff $\Lambda = 400$ MeV are much more satisfactory in the sense that the contribution from the residual three-body part w to the binding energy per particle is considerably smaller, and at the order of 0.5 MeV or less for the densities considered. Likewise, the results obtained with the non-local regulator at the cutoff 500 MeV are also satisfactory in the sense that the contribution from the residual 3NF w is at most 1 MeV to the energy per particle at densities beyond the saturation point. One might speculate whether this problematic feature of the local regulator with a cutoff 500 MeV is related to the large cutoff dependence found in finite nuclei using this regulator [69]. Naively one would expect that regulator dependencies are higher-order corrections in an EFT. The large scheme dependencies observed in Fig. 14 might therefore suggest that the cutoff $\Lambda = 500$ MeV is too close to the EFT breakdown scale.

For local and nonlocal regulators we considerably underbind nuclear matter. The saturation density for the local regulators is too high, while for the nonlocal regulator the saturation density is closer to the empirical value. We tried to adjust the LECs c_E and c_D such that an acceptable result could be obtained simultaneously for the saturation point in symmetric nuclear matter and the triton binding energy. For the nonlocal regulator the result is shown in Fig. 15. The blue band shows the region where the triton binding energy is reproduced within 5%. The red band shows the region where the saturation
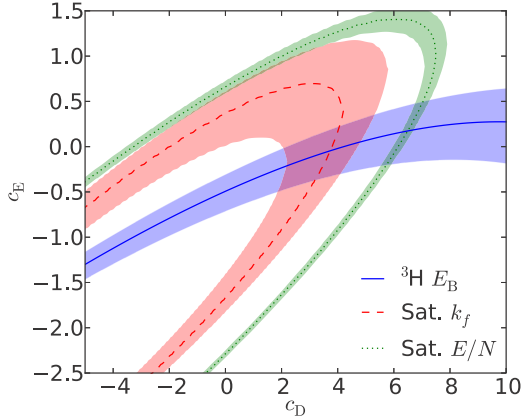
FIG. 15. (Color online) The blue band shows the region where the triton binding energy is reproduced within 5% of the experimental value. The red band shows the region where the saturation fermi momentum in symmetric nuclear matter is reproduced within 5% of its empirical value, and the green band shows the region where the energy per nucleon is within 5% of the empirical value.
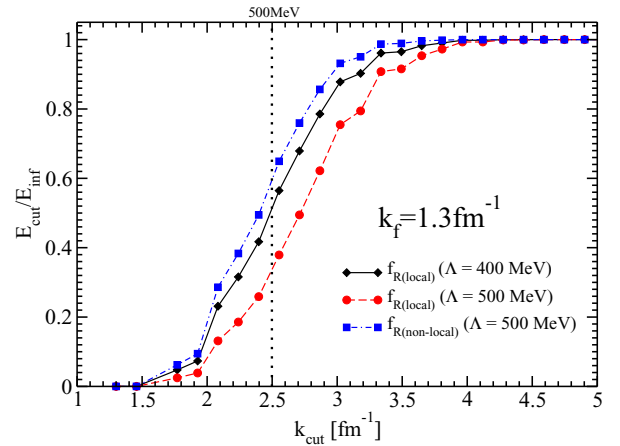

FIG. 16. (Color online) Cutoff dependent fraction of the residual 3NF contribution to the MBPT2 energy per particle in symmetric nuclear matter for different regulators. Results are shown for the local regulator with $\Lambda = 500$ MeV (diamonds), the local regulator with $\Lambda = 400$ MeV (squares), and for the non-local regulator with $\Lambda = 500$ MeV (circles). Calculations used 132 nucleons, $n_{\max} = 4$, and PBC.

Fermi momentum is within 5% of its empirical value, and the green band shows the region where the energy per nucleon is within 5% of the empirical value. The nuclear matter calculations were obtained from MBPT2 calculations using 28 nucleons, and we accounted for about 1 MeV per nucleon in missing correlations energy, and about 0.5 MeV per nucleon due to finite size effects. It thus seems that a simultaneous reproduction of saturation in light nuclei and infinite matter is not possible without adjusting other LECs. As an example we considered the point $c_E = 0.3$ and $c_D = -2.0$. This yields the saturation point $k_F \approx 1.4$ fm^{-1} and $E/A \approx 15.5$ MeV, while the triton binding energy is -13.53 MeV.

We would like to understand better the role that different regulators and cutoffs play for the chiral 3NF. Unfortunately, it is difficult to visualize 3NFs in momentum space [82,83]. We therefore compute the MBPT2 contribution of the residual 3NF w and cut off the involved momentum integrations at a single-particle momentum $k_{\rm cut}$. Figure 16 shows the fractional contribution of the MBPT2 energy correction of the residual 3NF as a function of $k_{\rm cut}$ at the Fermi momentum $k_F = 1.3$ fm^{-1}. The chiral cutoff of $\Lambda = 500$ MeV is also shown as a dashed line for comparison. We see that for the local cutoff $\Lambda = 500$ MeV most contributions to the MBPT2 result are from high single-particle momenta that are well above the nominal chiral cutoff. The situation is improved for the local regulator with lower cutoff $\Lambda = 400$ MeV and even more so for the nonlocal regulator with cutoff $\Lambda = 500$ MeV. For a discussion of different cutoff schemes and convergence issues in calculations of the homogeneous electron gas see Ref. [54].

Let us finally note that issues with 3NFs also arose in other calculations. Lovato *et al.* [29] pointed out that the equivalence of different chiral 3NF contact terms [40] is spoiled by local regulators. Roth *et al.* [84] used SRG evolution to soften the chiral NN interaction of Ref. [85] combined with the local 3NF of Ref. [62], and found that the results in medium-mass nuclei depend considerably on the SRG evolution scale. This dependence is reduced for a cutoff $\Lambda = 400$ MeV in the local

3NF [69]. Clearly, more studies of chiral 3NFs are necessary to fully understand regularization scheme dependences.

IV. SUMMARY

We have performed coupled-cluster calculations of nucleonic matter with interactions from chiral EFT at NNLO. The single-particle states consist of a discrete lattice in momentum space, and the implementation of twist-averaged boundary conditions mitigates shell oscillations and finite-size effects. Our benchmark calculations agree well with other well established methods. We find that neutron matter is perturbative, while symmetric nuclear matter is not perturbative, with significant contributions beyond perturbation theory and particle ladders.

For the employed NN potential NNLO$_{\rm opt}$ and 3NFs, the neutron matter results fall within the error estimates of previous calculations for chiral interactions, with 3NFs acting repulsively. For nuclear matter, the empirical saturation could not be reproduced, and the results are very sensitive to the employed regulator (local vs nonlocal) and cutoff. At larger chiral cutoffs, the nonlocal regulator is preferred over the local one because it corresponds closer to the cutoff generated by the finite single-particle basis. It seems that the variation of the 3NF contact terms alone is insufficient to achieve both an acceptable saturation point of nuclear matter and an acceptable binding of light nuclei.

[1] A. Burrows, Rev. Mod. Phys. **85**, 245 (2013).
[2] F. Weber, *Pulsars as Astrophysical Laboratories for Nuclear and Particle Physics* (IOP, London, 1999).
[3] H. Heiselberg and M. Hjorth-Jensen, Phys. Rep. **328**, 237 (2000).
[4] J. M. Lattimer and M. Prakash, Phys. Rep. **442**, 109 (2007).
[5] F. Sammarruca, Int. J. Mod. Phys. E **19**, 1259 (2010).
[6] J. M. Lattimer, Annu. Rev. Nucl. Part. Sci. **62**, 485 (2012).
[7] K. Hebeler, J. M. Lattimer, C. J. Pethick, and A. Schwenk, Astrophys. J. **773**, 11 (2013).
[8] B. A. Brown, Phys. Rev. Lett. **85**, 5296 (2000).
[9] C. J. Horowitz and J. Piekarewicz, Phys. Rev. Lett. **86**, 5647 (2001).
[10] S. Gandolfi, J. Carlson, and S. Reddy, Phys. Rev. C **85**, 032801 (2012).
[11] M. B. Tsang, J. R. Stone, F. Camera, P. Danielewicz, S. Gandolfi, K. Hebeler, C. J. Horowitz, J. Lee, W. G. Lynch, Z. Kohley *et al.*, Phys. Rev. C **86**, 015803 (2012).
[12] A. W. Steiner and S. Gandolfi, Phys. Rev. Lett. **108**, 081102 (2012).
[13] S. Shlomo and D. H. Youngblood, Phys. Rev. C **47**, 529 (1993).
[14] S. Abrahamyan, Z. Ahmed, H. Albataineh, K. Aniol, D. S. Armstrong, W. Armstrong, T. Averett, B. Babineau, A. Barbieri, V. Bellini *et al.* (PREX Collaboration), Phys. Rev. Lett. **108**, 112502 (2012).
[15] P.-G. Reinhard, J. Piekarewicz, W. Nazarewicz, B. K. Agrawal, N. Paar, and X. Roca-Maza, Phys. Rev. C **88**, 034325 (2013).
[16] J. Erler, C. J. Horowitz, W. Nazarewicz, M. Rafalski, and P.-G. Reinhard, Phys. Rev. C **87**, 044320 (2013).
[17] M. Kortelainen, T. Lesinski, J. Moré, W. Nazarewicz, J. Sarich, N. Schunck, M. V. Stoitsov, and S. Wild, Phys. Rev. C **82**, 024313 (2010).
[18] D. Lunney, J. M. Pearson, and C. Thibault, Rev. Mod. Phys. **75**, 1021 (2003).
[19] B. D. Day, Rev. Mod. Phys. **39**, 719 (1967).
[20] K. A. Brueckner, C. A. Levinson, and H. M. Mahmoud, Phys. Rev. **95**, 217 (1954).
[21] K. A. Brueckner, Phys. Rev. **100**, 36 (1955).
[22] M. Baldo and G. F. Burgio, Rep. Prog. Phys. **75**, 026301 (2012).
[23] M. Baldo, A. Polls, A. Rios, H.-J. Schulze, and I. Vidaña, Phys. Rev. C **86**, 064001 (2012).
[24] H. Kümmel, K. H. Lührmann, and J. G. Zabolitzky, Phys. Rep. **36**, 1 (1978).
[25] B. D. Day and G. Zabolitzky, Nucl. Phys. A **366**, 221 (1981).
[26] J. Carlson, J. Morales, V. R. Pandharipande, and D. G. Ravenhall, Phys. Rev. C **68**, 025802 (2003).
[27] S. Gandolfi, A. Y. Illarionov, K. E. Schmidt, F. Pederiva, and S. Fantoni, Phys. Rev. C **79**, 054005 (2009).
[28] A. Gezerlis and J. Carlson, Phys. Rev. C **81**, 025803 (2010).
[29] A. Lovato, O. Benhar, S. Fantoni, and K. E. Schmidt, Phys. Rev. C **85**, 024003 (2012).
[30] A. Gezerlis, I. Tews, E. Epelbaum, S. Gandolfi, K. Hebeler, A. Nogga, and A. Schwenk, Phys. Rev. Lett. **111**, 032501 (2013).
[31] W. Dickhoff and C. Barbieri, Prog. Part. Nucl. Phys. **52**, 377 (2004).
[32] V. Somà and P. Bożek, Phys. Rev. C **78**, 054003 (2008).
[33] A. Rios and V. Somà, Phys. Rev. Lett. **108**, 012501 (2012).
[34] A. Carbone, A. Polls, and A. Rios, Phys. Rev. C **88**, 044302 (2013).
[35] G. Baardsen, A. Ekström, G. Hagen, and M. Hjorth-Jensen, Phys. Rev. C **88**, 054312 (2013).
[36] A. Ekström, G. Baardsen, C. Forssén, G. Hagen, M. Hjorth-Jensen, G. R. Jansen, R. Machleidt, W. Nazarewicz, T. Papenbrock, J. Sarich *et al.*, Phys. Rev. Lett. **110**, 192502 (2013).
[37] R. Machleidt and D. Entem, Phys. Rep. **503**, 1 (2011).
[38] E. Epelbaum, H.-W. Hammer, and U.-G. Meißner, Rev. Mod. Phys. **81**, 1773 (2009).
[39] U. van Kolck, Phys. Rev. C **49**, 2932 (1994).
[40] E. Epelbaum, A. Nogga, W. Glöckle, H. Kamada, U.-G. Meißner, and H. Witała, Phys. Rev. C **66**, 064001 (2002).
[41] E. Epelbaum, H. Krebs, D. Lee, and U.-G. Meißner, Euro. Phys. J. A **40**, 199 (2009).
[42] K. Hebeler and A. Schwenk, Phys. Rev. C **82**, 014314 (2010).
[43] K. Hebeler, S. K. Bogner, R. J. Furnstahl, A. Nogga, and A. Schwenk, Phys. Rev. C **83**, 031301 (2011).
[44] J. Holt, N. Kaiser, and W. Weise, Nucl. Phys. A **876**, 61 (2012).
[45] H.-W. Hammer, A. Nogga, and A. Schwenk, Rev. Mod. Phys. **85**, 197 (2013).
[46] T. Krüger, I. Tews, K. Hebeler, and A. Schwenk, Phys. Rev. C **88**, 025802 (2013).
[47] L. Coraggio, J. W. Holt, N. Itaco, R. Machleidt, and F. Sammarruca, Phys. Rev. C **87**, 014322 (2013).
[48] C. Drischler, V. Somá, and A. Schwenk, arXiv:1310.5627.
[49] T. Inoue, S. Aoki, T. Doi, T. Hatsuda, Y. Ikeda, N. Ishii, K. Murano, H. Nemura, and K. Sasaki (HAL QCD Collaboration), Phys. Rev. Lett. **111**, 112503 (2013).
[50] D. J. Dean and M. Hjorth-Jensen, Phys. Rev. C **69**, 054320 (2004).
[51] K. Kowalski, D. J. Dean, M. Hjorth-Jensen, T. Papenbrock, and P. Piecuch, Phys. Rev. Lett. **92**, 132501 (2004).
[52] R. J. Bartlett and M. Musiał, Rev. Mod. Phys. **79**, 291 (2007).

[53] I. Shavitt and R. J. Bartlett, *Many-body Methods in Chemistry and Physics* (Cambridge University Press, Cambridge, 2009).

[54] J. J. Shepherd, A. Grüneis, G. H. Booth, G. Kresse, and A. Alavi, Phys. Rev. B **86**, 035111 (2012).

[55] A. Roggero, A. Mukherjee, and F. Pederiva, Phys. Rev. B **88**, 115138 (2013).

[56] F. E. Harris, H. J. Monkhorst, and D. L. Freeman, *Algebraic and Diagrammatic Methods in Many-Fermion Theory* (Oxford University Press, Oxford, 1992).

[57] D. L. Freeman, Phys. Rev. B **15**, 5512 (1977).

[58] R. F. Bishop and K. H. Lührmann, Phys. Rev. B **17**, 3757 (1978).

[59] C. Gros, Zeitschrift für Physik B Condensed Matter **86**, 359 (1992).

[60] C. Gros, Phys. Rev. B **53**, 6865 (1996).

[61] C. Lin, F. H. Zong, and D. M. Ceperley, Phys. Rev. E **64**, 016702 (2001).

[62] P. Navrátil, Few-Body Syst. **41**, 117 (2007).

[63] P. Navrátil, S. Quaglioni, and D. Gazit (private communication).

[64] G. Hagen, T. Papenbrock, D. J. Dean, A. Schwenk, A. Nogga, M. Włoch, and P. Piecuch, Phys. Rev. C **76**, 034302 (2007).

[65] S. Binder, P. Piecuch, A. Calci, J. Langhammer, P. Navrátil, and R. Roth, Phys. Rev. C **88**, 054319 (2013).

[66] G. Hagen, T. Papenbrock, D. J. Dean, and M. Hjorth-Jensen, Phys. Rev. Lett. **101**, 092502 (2008).

[67] G. Hagen, T. Papenbrock, D. J. Dean, and M. Hjorth-Jensen, Phys. Rev. C **82**, 034330 (2010).

[68] S. K. Bogner, R. J. Furnstahl, and R. J. Perry, Phys. Rev. C **75**, 061001 (2007).

[69] R. Roth, S. Binder, K. Vobig, A. Calci, J. Langhammer, and P. Navrátil, Phys. Rev. Lett. **109**, 052501 (2012).

[70] K. Raghavachari, J. Chem. Phys. **82**, 4607 (1985).

[71] B. D. Day, Rev. Mod. Phys. **50**, 495 (1978).

[72] B. D. Day, Phys. Rev. C **24**, 1203 (1981).

[73] M. I. Haftel and F. Tabakin, Nucl. Phys. A **158**, 1 (1970).

[74] K. Suzuki, R. Okamoto, M. Kohno, and S. Nagata, Nucl. Phys. A **665**, 92 (2000).

[75] K. A. Brueckner and J. L. Gammel, Phys. Rev. **109**, 1023 (1958).

[76] K. Schmidt and S. Fantoni, Phys. Lett. B **446**, 99 (1999).

[77] D. Thompson, M. Lemere, and Y. Tang, Nucl. Phys. A **286**, 53 (1977).

[78] S. Gandolfi, A. Y. Illarionov, F. Pederiva, K. E. Schmidt, and S. Fantoni, Phys. Rev. C **80**, 045802 (2009).

[79] C. Horowitz and A. Schwenk, Nucl. Phys. A **776**, 55 (2006).

[80] Y. S. Lee and R. J. Bartlett, J. Chem. Phys. **80**, 4371 (1984).

[81] Y. S. Lee, S. A. Kucharski, and R. J. Bartlett, J. Chem. Phys. **81**, 5906 (1984).

[82] K. Hebeler, Phys. Rev. C **85**, 021002 (2012).

[83] K. A. Wendt, Phys. Rev. C **87**, 061001 (2013).

[84] R. Roth, J. Langhammer, A. Calci, S. Binder, and P. Navrátil, Phys. Rev. Lett. **107**, 072501 (2011).

[85] D. R. Entem and R. Machleidt, Phys. Rev. C **68**, 041001 (2003).